

Relativistic Hartree-Bogoliubov description of the neutron drip-line in light nuclei

G.A. Lalazissis, D. Vretenar, W. Pöschl and P. Ring
Physik-Department der Technischen Universität München,
D-85747 Garching, Germany

September 4, 2018

Abstract

The Relativistic Hartree Bogoliubov theory is applied in the mean-field approximation to the description of properties of light nuclei with large neutron excess. Pairing correlations and the coupling to particle continuum states are described by finite range two-body forces. Using standard parameter sets for the mean-field Lagrangian and the pairing interaction of Gogny-type, self-consistent solutions in coordinate space are calculated for the ground states of a number of neutron-rich nuclei. The model predicts the location of the neutron drip-line, reduction of the spin-orbit interaction, *rms* radii, changes in surface properties, the formation of neutron skin and of neutron halo.

1 Introduction

Experimental and theoretical studies of exotic nuclei with extreme isospin values present one of the most active areas of research in nuclear physics. Experiments with radioactive nuclear beams provide the opportunity to study very short-lived nuclei with extreme neutron to proton ratio N/Z . New theoretical models and techniques are being developed in order to describe unique phenomena in nuclei very different from those usually encountered along the line of stability. On the neutron-rich side in particular, exotic phenomena include the weak binding of the outermost neutrons, pronounced effects of coupling between bound states and the particle continuum, regions of neutron halos with very diffuse neutron densities and major modifications of the shell structures. Neutron drip lines of relatively light nuclei have become accessible in experiments, and properties of these exotic objects are currently being studied with a variety of theoretical approaches. Because of their relevance to the r-process in nucleosynthesis, nuclei close to the neutron drip line are also very important in nuclear astrophysics. Detailed knowledge of their structure and properties would help the determination of astrophysical conditions for the formation of neutron rich stable isotopes.

The main problem in the theoretical description of drip-line nuclei arises from the closeness of the Fermi level to the particle continuum: particle-hole and pair excitations reach the continuum. The coupling between bound states and the particle continuum has to be explicitly included in any model description. The Relativistic Hartree Bogoliubov (RHB) theory, which is a relativistic extension of the Hartree Fock Bogoliubov theory, provides a unified description of mean-field and pairing correlations. A fully self-consistent RHB theory in coordinate space correctly describes the coupling between

bound and continuum states. The theory provides a framework for describing the nuclear many-body problem as a relativistic system of baryons and mesons. In the self-consistent mean-field approximation, the theory has been used to perform detailed calculations for a variety of nuclear structure phenomena, as well as for the dynamics of heavy-ion collisions. Although conventional non-relativistic Hartree-Fock models and the relativistic mean-field theory predict very similar properties for nuclei close to the β -stability line, recent applications to the structure of drip-line nuclei have shown significant differences, especially in the isospin dependence of the spin-orbit potential.

In Refs. [1, 2] we have investigated, in the framework of relativistic Hartree-Bogoliubov theory, light nuclear systems with large neutron excess. The isospin dependence of the spin-orbit interaction in light neutron-rich nuclei has been studied in Ref. [2]. In [1] we have described the microscopic details of the formation of neutron halo in the mass region above the $s-d$ shell. Pairing correlations and the coupling to particle continuum states have been described by finite range two-body Gogny-type interaction. Finite element methods have been used in the coordinate space discretization of the coupled system of Dirac-Hartree-Bogoliubov and Klein-Gordon equations [3, 4]. Calculations have been performed for the isotopic chains of Ne and C nuclei. We find evidence for the occurrence of multi-neutron halo in heavier Ne isotopes. The detailed microscopic analysis has shown how the properties of the 1f-2p orbitals near the Fermi level and the neutron pairing interaction determine the formation of the halo. On the other hand our calculations have shown that, although for Ne the neutron drip was found at $N = 32$, for C already the $N = 20$ isotope is unbound. Preliminary results for Oxygen have placed the neutron drip at $N = 18$ or $N = 20$, depending

on the effective force used in the mean-field calculations. This is a very interesting result: by adding just one or two protons, the resulting mean-fields bind up to twelve more neutrons.

In the present work we extend our investigation of Ref. [1], and study in detail the neutron drip-line for the elements C, N, O, F, Ne, Na and Mg. In the region around $N = 20$ we expect that these nuclei are to a good approximation spherical, or that an eventual small deformation would not change our results quantitatively. In particular, we study how the proton number affects the neutron single-particle levels around $N = 20$ and the position of the neutron drip. We also discuss changes in the spin-orbit interaction, surface diffuseness and the formation of the neutron halo. In Sec. 2 we present an outline of the relativistic Hartree-Bogoliubov theory and discuss the various approximations. In Sec. 3 the theory is applied to the calculation of ground state properties of a number of light neutron-rich nuclei. A summary of our results is presented in Sec. 4.

2 The relativistic Hartree-Bogoliubov model

Detailed properties of nuclear matter and finite nuclei along the β -stability line have been very successfully described in the framework of relativistic mean field models [5, 6, 7, 8]. In comparison with conventional non-relativistic approaches, relativistic models explicitly include mesonic degrees of freedom and describe the nucleons as Dirac particles. Nucleons interact in a relativistic covariant manner through the exchange of virtual mesons: the isoscalar scalar σ -meson, the isoscalar vector ω -meson and the isovector vector ρ -meson. The model is based on the one boson exchange description of the nucleon-nucleon interaction. We start from the effective Lagrangian

density

$$\begin{aligned}
\mathcal{L} = & \bar{\psi} (i\gamma \cdot \partial - m) \psi \\
& + \frac{1}{2}(\partial\sigma)^2 - U(\sigma) - \frac{1}{4}\Omega_{\mu\nu}\Omega^{\mu\nu} + \frac{1}{2}m_\omega^2\omega^2 - \frac{1}{4}\vec{R}_{\mu\nu}\vec{R}^{\mu\nu} + \frac{1}{2}m_\rho^2\vec{\rho}^2 - \frac{1}{4}F_{\mu\nu}F^{\mu\nu} \\
& - g_\sigma\bar{\psi}\sigma\psi - g_\omega\bar{\psi}\gamma \cdot \omega\psi - g_\rho\bar{\psi}\gamma \cdot \vec{\rho}\vec{\tau}\psi - e\bar{\psi}\gamma \cdot A\frac{(1 - \tau_3)}{2}\psi .
\end{aligned} \tag{1}$$

Vectors in isospin space are denoted by arrows, and bold-faced symbols will indicate vectors in ordinary three-dimensional space. The Dirac spinor ψ denotes the nucleon with mass m . m_σ , m_ω , and m_ρ are the masses of the σ -meson, the ω -meson, and the ρ -meson. g_σ , g_ω , and g_ρ are the corresponding coupling constants for the mesons to the nucleon. $e^2/4\pi = 1/137.036$. Coupling constants and unknown meson masses are parameters, adjusted to fit data on nuclear matter and finite nuclei. $U(\sigma)$ denotes the non-linear σ self-interaction [9]

$$U(\sigma) = \frac{1}{2}m_\sigma^2\sigma^2 + \frac{1}{3}g_2\sigma^3 + \frac{1}{4}g_3\sigma^4, \tag{2}$$

and $\Omega^{\mu\nu}$, $\vec{R}^{\mu\nu}$, and $F^{\mu\nu}$ are field tensors

$$\Omega^{\mu\nu} = \partial^\mu\omega^\nu - \partial^\nu\omega^\mu \tag{3}$$

$$\vec{R}^{\mu\nu} = \partial^\mu\vec{\rho}^\nu - \partial^\nu\vec{\rho}^\mu \tag{4}$$

$$F^{\mu\nu} = \partial^\mu A^\nu - \partial^\nu A^\mu. \tag{5}$$

The lowest order of the quantum field theory is the *mean-field* approximation: the meson field operators are replaced by their expectation values. The A nucleons, described by a Slater determinant $|\Phi\rangle$ of single-particle spinors ψ_i , ($i = 1, 2, \dots, A$), move independently in the classical meson fields. The sources of the meson fields are defined by the nucleon densities and currents. The ground state of a nucleus is described by the stationary self-consistent

solution of the coupled system of Dirac and Klein-Gordon equations. In the static case for an even-even system, there will be no currents in the nucleus, and the spatial vector components $\boldsymbol{\omega}$, $\boldsymbol{\rho}_3$ and \mathbf{A} vanish. The Dirac equation reads

$$\left\{ -i\boldsymbol{\alpha} \cdot \boldsymbol{\nabla} + \beta(m + g_\sigma\sigma) + g_\omega\omega^0 + g_\rho\tau_3\rho_3^0 + e\frac{(1-\tau_3)}{2}A^0 \right\} \psi_i = \varepsilon_i\psi_i \quad (6)$$

The effective mass $m^*(\mathbf{r})$ is defined

$$m^*(\mathbf{r}) = m + g_\sigma\sigma(\mathbf{r}), \quad (7)$$

and the potential $V(\mathbf{r})$

$$V(\mathbf{r}) = g_\omega\omega^0(\mathbf{r}) + g_\rho\tau_3\rho_3^0(\mathbf{r}) + e\frac{(1-\tau_3)}{2}A^0(\mathbf{r}). \quad (8)$$

In order to describe ground-state properties of spherical open-shell nuclei, pairing correlations have to be taken into account. For nuclei close to the β -stability line, pairing has been included in the relativistic mean-field model in the form of a simple BCS approximation [10]. However, for nuclei far from stability the BCS model presents only a poor approximation. In particular, in drip-line nuclei the Fermi level is found close to the particle continuum. The lowest particle-hole or particle-particle modes are often embedded in the continuum, and the coupling between bound and continuum states has to be taken into account explicitly. The BCS model does not provide a correct description of the scattering of nucleonic pairs from bound states to the positive energy continuum [11, 12]. It leads to an unbound system, because levels in the continuum are partially occupied. Including the system in a box of finite size leads to unreliable predictions for nuclear radii depending on the size of this box. In the non-relativistic case, a unified description of mean-field and pairing correlations is obtained in the framework of the Hartree-Fock-Bogoliubov (HFB) theory in coordinate space [11]. The ground state of a

nucleus $|\Phi\rangle$ is represented as the vacuum with respect to independent quasi-particles. The quasi-particle operators are defined by a unitary Bogoliubov transformation of the single-nucleon creation and annihilation operators. The generalized single-particle Hamiltonian of HFB theory contains two average potentials: the self-consistent field $\hat{\Gamma}$ which encloses all the long range ph correlations, and a pairing field $\hat{\Delta}$ which sums up the pp -correlations. The expectation value of the nuclear Hamiltonian $\langle \Phi | \hat{H} | \Phi \rangle$ can be expressed as a function of the hermitian density matrix ρ , and the antisymmetric pairing tensor κ . The variation of the energy functional with respect to ρ and κ produces the single quasi-particle Hartree-Fock-Bogoliubov equations [13]

$$\begin{pmatrix} \hat{h} - \lambda & \hat{\Delta} \\ -\hat{\Delta}^* & -\hat{h} + \lambda \end{pmatrix} \begin{pmatrix} U_k \\ V_k \end{pmatrix} = E_k \begin{pmatrix} U_k \\ V_k \end{pmatrix}. \quad (9)$$

HFB-theory, being a variational approximation, results in a violation of basic symmetries of the nuclear system, among which the most important is the non conservation of the number of particles. In order that the expectation value of the particle number operator in the ground state equals the number of nucleons, equations (9) contain a chemical potential λ which has to be determined by the particle number subsidiary condition. The column vectors denote the quasi-particle wave functions, and E_k are the quasi-particle energies.

If the pairing field $\hat{\Delta}$ is a constant, HFB reduces to the BCS-approximation. The lower and upper components $U_k(r)$ and $V_k(r)$ are proportional, with the BCS-occupation amplitudes as proportionality constants. For a more general pairing interaction this will no longer be the case. As opposed to the functions $U_k(r)$, the lower components $V_k(r)$ are localized functions of \mathbf{r} , as long as the chemical potential λ is below the continuum limit. Since the densities are bilinear products of $V_k(r)$ (see Eqs.(15)-(18)), the system is always

localized. According to the theorem of Bloch and Messiah [13], an HFB wave function can be written either in the quasiparticle basis as a product of independent quasi-particle states, or in the *canonical basis* as a highly correlated BCS-state. In the *canonical basis* nucleons occupy single-particle states. If the chemical potential is close to the continuum, the pairing interaction scatters pairs of nucleons into continuum states. Because of additional pairing correlations, particles which occupy those levels cannot evaporate. Mathematically this is expressed by an additional non-trivial transformation which connects the particle operators in the canonical basis to the quasi-particles of the HFB wave function.

The relativistic extension of the HFB theory was introduced in Ref. [14]. In the Hartree approximation for the self-consistent mean field, the Relativistic Hartree-Bogoliubov (RHB) equations read

$$\begin{pmatrix} \hat{h}_D - m - \lambda & \hat{\Delta} \\ -\hat{\Delta}^* & -\hat{h}_D + m + \lambda \end{pmatrix} \begin{pmatrix} U_k(\mathbf{r}) \\ V_k(\mathbf{r}) \end{pmatrix} = E_k \begin{pmatrix} U_k(\mathbf{r}) \\ V_k(\mathbf{r}) \end{pmatrix}. \quad (10)$$

where \hat{h}_D is the single-nucleon Dirac Hamiltonian(6), and m is the nucleon mass. The RHB equations have to be solved self-consistently, with potentials determined in the mean-field approximation from solutions of Klein-Gordon equations

$$[-\Delta + m_\sigma^2] \sigma(\mathbf{r}) = -g_\sigma \rho_s(\mathbf{r}) - g_2 \sigma^2(\mathbf{r}) - g_3 \sigma^3(\mathbf{r}) \quad (11)$$

$$[-\Delta + m_\omega^2] \omega^0(\mathbf{r}) = -g_\omega \rho_v(\mathbf{r}) \quad (12)$$

$$[-\Delta + m_\rho^2] \rho^0(\mathbf{r}) = -g_\rho \rho_3(\mathbf{r}) \quad (13)$$

$$-\Delta A^0(\mathbf{r}) = e \rho_p(\mathbf{r}). \quad (14)$$

for the sigma meson, omega meson, rho meson and photon field, respectively. The spatial components ω , ρ , and \mathbf{A} vanish due to time reversal symmetry. Because of charge conservation, only the 3-component of the isovector rho

meson contributes. The source terms in equations (11) to (14) are sums of bilinear products of baryon amplitudes

$$\rho_s(\mathbf{r}) = \sum_{E_k>0} V_k^\dagger(\mathbf{r})\gamma^0 V_k(\mathbf{r}), \quad (15)$$

$$\rho_v(\mathbf{r}) = \sum_{E_k>0} V_k^\dagger(\mathbf{r})V_k(\mathbf{r}), \quad (16)$$

$$\rho_3(\mathbf{r}) = \sum_{E_k>0} V_k^\dagger(\mathbf{r})\tau_3 V_k(\mathbf{r}), \quad (17)$$

$$\rho_{em}(\mathbf{r}) = \sum_{E_k>0} V_k^\dagger(\mathbf{r})\frac{1-\tau_3}{2}V_k(\mathbf{r}). \quad (18)$$

where the sums run over all positive energy states. For M degrees of freedom, for example number of nodes on a radial mesh, the HB equations are $2M$ -dimensional and have $2M$ eigenvalues and eigenvectors. To each eigenvector (U_k, V_k) with eigenvalue E_k , there corresponds an eigenvector (V_k^*, U_k^*) with eigenvalue $-E_k$. Since baryon quasi-particle operators satisfy fermion commutation relations, it is forbidden to occupy the levels E_k and $-E_k$ simultaneously. Usually one chooses the M positive eigenvalues E_k for the solution that corresponds to a ground state of a nucleus with even particle number.

The system of equations (10), and (11) to (14), is solved self-consistently in coordinate space by discretization on the finite element mesh [3, 4]. In the coordinate space representation of the pairing field $\hat{\Delta}$ in (10), the kernel of the integral operator is

$$\Delta_{ab}(\mathbf{r}, \mathbf{r}') = \frac{1}{2} \sum_{c,d} V_{abcd}(\mathbf{r}, \mathbf{r}')\kappa_{cd}(\mathbf{r}, \mathbf{r}'). \quad (19)$$

where a, b, c, d denote all quantum numbers, apart from the coordinate \mathbf{r} , that specify the single-nucleon states. $V_{abcd}(\mathbf{r}, \mathbf{r}')$ are matrix elements of a general two-body pairing interaction, and the pairing tensor is defined as

$$\kappa_{cd}(\mathbf{r}, \mathbf{r}') = \sum_{E_k>0} U_{ck}^*(\mathbf{r})V_{dk}(\mathbf{r}'). \quad (20)$$

The integral operator $\hat{\Delta}$ acts on the wave function $V_k(\mathbf{r})$:

$$(\hat{\Delta}V_k)(\mathbf{r}) = \sum_b \int d^3r' \Delta_{ab}(\mathbf{r}, \mathbf{r}') V_{bk}(\mathbf{r}'). \quad (21)$$

The eigensolutions of Eq. (10) form a set of orthogonal (normalized) single quasi-particle states. The corresponding eigenvalues are the single quasi-particle energies. In the self-consistent iteration procedure we work in the basis of quasi-particle states. The self-consistent quasi-particle eigenspectrum is then transformed into the canonical basis of single-particle states. The canonical basis is defined to be the one in which the matrix $R_{kk'} = \langle V_k(\mathbf{r}) | V_{k'}(\mathbf{r}) \rangle$ is diagonal. The transformation to the canonical basis determines the energies and occupation probabilities of single-particle states, that correspond to the self-consistent solution for the ground state of a nucleus.

For nuclear systems with spherical symmetry the fields $\sigma(r)$, $\omega^0(r)$, $\rho^0(r)$, and $A^0(r)$ depend only on the radial coordinate r . The nucleon spinors U_k (V_k) in (10) are characterized by the angular momentum j , its z -projection m , parity π and the isospin $t_3 = \pm \frac{1}{2}$ for neutron and proton. The two Dirac spinors $U_k(\mathbf{r})$ and $V_k(\mathbf{r})$ form a *super-spinor*

$$\Phi_k(\mathbf{r}) = \begin{pmatrix} U_k(\mathbf{r}) \\ V_k(\mathbf{r}) \end{pmatrix} \quad (22)$$

where

$$U_k(V_k)(\mathbf{r}, s, t_3) = \begin{pmatrix} g_{U(V)}(r) \Omega_{j,l,m}(\theta, \varphi, s) \\ i f_{U(V)}(r) \Omega_{j,\tilde{l},m}(\theta, \varphi, s) \end{pmatrix} \chi_\tau(t_3). \quad (23)$$

$g(r)$ and $f(r)$ are radial amplitudes, χ_τ is the isospin function, the orbital angular momenta l and \tilde{l} are determined by j and the parity π

$$l = \begin{cases} j + 1/2 & \text{for } \pi = (-1)^{j+1/2} \\ j - 1/2 & \text{for } \pi = (-1)^{j-1/2} \end{cases}, \quad (24)$$

and

$$\tilde{l} = \begin{cases} j - 1/2 & \text{for } \pi = (-1)^{j+1/2} \\ j + 1/2 & \text{for } \pi = (-1)^{j-1/2} \end{cases} \quad (25)$$

Ω_{jlm} is the tensor product of the orbital and spin functions

$$\Omega_{j,l,m}(\theta, \varphi, s) = \sum_{m_s, m_l} \langle \frac{1}{2} m_s l m_l | j m \rangle \chi_{\frac{1}{2} m_s} Y_{lm_l}(\theta, \varphi). \quad (26)$$

It is useful to define a single angular quantum number κ as the eigenvalue of the operator $(1 + \hat{\sigma} \cdot \hat{\mathbf{1}})$

$$(1 + \hat{\sigma} \cdot \hat{\mathbf{1}}) \Omega_{\kappa, m} = -\kappa \Omega_{\kappa, m}, \quad (27)$$

$$\kappa = \pm(j + 1/2) \quad \text{for} \quad j = l \mp 1/2. \quad (28)$$

$\kappa = \pm 1, \pm 2, \pm 3, \dots$. The equations for the radial amplitudes $g_{U(V)}(r)$ and $f_{U(V)}(r)$ are derived from Eq. (10). The radial single-particle Dirac Hamiltonian reads

$$\hat{h}_D(r) = \sigma_3 \sigma_1 (\partial_r + r^{-1}) - \sigma_1 \kappa r^{-1} + \sigma_3 m + \sigma_3 S(r) + V_0(r), \quad (29)$$

where the scalar and vector potentials are

$$S(r) = g_\sigma \sigma(r), \quad \text{and} \quad V^0(r) = g_\omega \omega^0(r) + g_\rho \tau_3 \rho_3^0(r) + e \frac{(1 - \tau_3)}{2} A^0(r). \quad (30)$$

σ_i ($i=1,2,3$) are the Pauli matrices. The integral operator of the pairing interaction takes the form

$$\hat{\Delta}(r) = \int_0^\infty dr' r'^2 \Delta(r, r') \quad (31)$$

The kernel of the integral operator is defined

$$\Delta_{aa'}^{JM}(r, r') = \frac{1}{2} \sum_{\tilde{a}, \tilde{a}'} \langle r a, r' a' | \hat{V} | r \tilde{a}, r' \tilde{a}' \rangle_{JM} \kappa_{\tilde{a}, \tilde{a}'}(r, r') \quad (32)$$

where r and r' denote radial coordinates, a, a', \tilde{a} and \tilde{a}' are quantum numbers that completely specify single-nucleon states: (n, l, j, m) or (n, κ, m) , J and M are the total angular momentum of the pair, and its z -projection,

respectively. In the particle-particle (pp) channel the pairing interaction is approximated by a two-body finite range Gogny interaction

$$V^{pp}(1, 2) = \sum_{i=1,2} e^{-((\mathbf{r}_1 - \mathbf{r}_2)/\mu_i)^2} (W_i + B_i P^\sigma - H_i P^\tau - M_i P^\sigma P^\tau), \quad (33)$$

with parameters μ_i , W_i , B_i , H_i and M_i ($i = 1, 2$). For the $J = 0$ contribution to the pairing matrix elements, the kernel of the integral operator reads

$$\Delta_\kappa(r, r') = \frac{1}{2} \sum_{\tilde{\kappa}} V_{\kappa\tilde{\kappa}}^{J=0}(r, r') \kappa_{\tilde{\kappa}}(r, r'). \quad (34)$$

The pairing tensor is calculated

$$\kappa_\kappa(r, r') = \sum_n 2|\kappa| \begin{pmatrix} g_{n,\kappa}^{(U)}(r) g_{n,\kappa}^{(V)}(r') & 0 \\ 0 & f_{n,\kappa}^{(U)}(r) f_{n,\kappa}^{(V)}(r') \end{pmatrix} \quad (35)$$

where, for a quantum number κ , the sum runs over all solutions in the specified energy interval $0 < E < E_{\max}$. If we define the Dirac spinors

$$\Phi_U(r) := \begin{pmatrix} g_U(r) \\ i f_U(r) \end{pmatrix} \quad \text{and} \quad \Phi_V(r) := \begin{pmatrix} g_V(r) \\ i f_V(r) \end{pmatrix}, \quad (36)$$

the radial Dirac-Hartree-Bogoliubov equations read

$$\begin{aligned} (\hat{h}_D(r) - m - \lambda) \Phi_U(r) + \int_0^\infty dr' r'^2 \Delta(r, r') \Phi_V(r') &= E \Phi_U(r) \\ (-\hat{h}_D(r) + m + \lambda) \Phi_V(r) + \int_0^\infty dr' r'^2 \Delta(r, r') \Phi_U(r') &= E \Phi_V(r) \end{aligned} \quad (37)$$

The meson and photon fields are solution of the Klein-Gordon equations

$$\left(-\partial_r^2 - \frac{2}{r} \partial_r + m_\sigma^2\right) \sigma(r) = -g_\sigma \rho_s(r) - g_2 \sigma^2(r) - g_3 \sigma^3(r) \quad (38)$$

$$\left(-\partial_r^2 - \frac{2}{r} \partial_r + m_\omega^2\right) \omega^0(r) = -g_\omega \rho_v(r) \quad (39)$$

$$\left(-\partial_r^2 - \frac{2}{r} \partial_r + m_\rho^2\right) \rho^0(r) = -g_\rho \rho_3(r) \quad (40)$$

$$\left(-\partial_r^2 - \frac{2}{r} \partial_r\right) A^0(r) = e \rho_p(r). \quad (41)$$

3 Neutron drip-line in light nuclei

The details of the neutron drip-line will depend on the single-particle levels, position of the Fermi energy, pairing interaction and coupling between bound and continuum states. In order to ascertain that our microscopic predictions do not crucially depend on the choice of the effective interaction, we perform calculations for three parameter sets of the mean-field Lagrangian: NL1 [15], NL3 [16], and NL-SH [17]. The effective forces NL1 and NL-SH have been frequently used to calculate properties of nuclear matter and of finite nuclei, and have become standard parameterizations for relativistic mean-field calculations. The parameter set NL3 has been derived recently [16] by fitting ground state properties of a large number of spherical nuclei. Properties calculated with the NL3 effective interaction are found to be in very good agreement with experimental data for nuclei at and away from the line of β -stability.

In the pairing channel one should in principle use a one-meson exchange interaction V_{abcd} derived by the elimination of the mesonic degrees of freedom in the Lagrangian (1). However, as it was shown in Ref. [14], the standard parameter sets of the mean-field approximation lead to completely unrealistic pairing matrix elements. These parameters do not reproduce the scattering data. Since at present a relativistic pairing force with parameters consistent with those of the mean-field potential is not available, we use a phenomenological Gogny-type finite range interaction in the pp -channel, a procedure which requires no cut-off and which provides a very reliable description of pairing properties in finite nuclei. The parameter set D1S [18] is used for the finite range Gogny type interaction.

In Ref. [1] we have studied in detail the formation of the neutron halo

in Ne isotopes. In order to be more complete and as an introduction to the discussion that follows, we briefly review the main arguments and results of that work. In Fig. 1a the *rms* radii for Ne isotopes are plotted as functions of neutron number. We display neutron and proton *rms* radii, and the $N^{1/3}$ curve normalized so that it coincides with the neutron radius in ^{20}Ne . The neutron *rms* radii follow the mean-field $N^{1/3}$ curve up to $N \approx 22$. For larger values of N the neutron radii display a sharp increase, while the proton radii stay practically constant. This sudden increase in neutron *rms* radii has been interpreted as evidence for the formation of a multi-particle halo. The phenomenon was also observed in the plot of proton and neutron density distributions. The proton density profiles do not change with the number of neutrons, while the neutron density distributions display an abrupt change between ^{30}Ne and ^{32}Ne . The microscopic origin of the neutron halo has been found in a delicate balance of the self-consistent mean-field and the pairing field. This is shown in Fig. 1b, where we display the neutron single-particle states $1f_{7/2}$, $2p_{3/2}$ and $2p_{1/2}$ in the canonical basis, and the Fermi energy as function of the neutron number. For $N \leq 22$ the triplet of states is high in the continuum, and the Fermi level uniformly increases toward zero. The triplet approaches zero energy, and a gap is formed between these states and all other states in the continuum. The shell structure dramatically changes at $N \geq 22$. Between $N = 22$ and $N = 32$ the Fermi level is practically constant and very close to the continuum. The addition of neutrons in this region of the drip does not increase the binding. Only the spatial extension of neutron distribution displays an increase. The formation of the neutron halo is related to the quasi-degeneracy of the triplet of states $1f_{7/2}$, $2p_{3/2}$ and $2p_{1/2}$. The pairing interaction promotes neutrons from the $1f_{7/2}$ orbital to the $2p$ levels.

Since these levels are so close in energy, the total binding energy does not change significantly. Due to their small centrifugal barrier, the $2p_{3/2}$ and $2p_{1/2}$ orbitals form the halo. The last bound isotope is ^{40}Ne . For $N \geq 32$ ($A \geq 42$) the neutron Fermi level becomes positive, and heavier isotopes are not bound any more. A similar mechanism has been studied in Ref. [19], for the experimentally observed halo in the nucleus ^{11}Li . There the formation of the halo is determined by the pair of neutron levels $1p_{1/2}$ and $2s_{1/2}$. A giant halo has been also predicted for Zirconium isotopes [20]. In that case the halo originates from the neutron orbitals $2f_{7/2}$, $3p_{3/2}$ and $3p_{1/2}$.

In Figs. 2, 3 and 4 we display the neutron single-particle energies in canonical basis for C, N, O, F, Ne, Na and Mg, in the region around neutron number $N=20$. In Figs. 2 and 3 the left hand side columns display results calculated with the NL1 effective interaction, NL3 results are shown in the central panels, and on the right hand side levels that correspond to the NL-SH parameterization are shown, as function of neutron number. For Carbon, in Fig. 4 we display results obtained with the NL3 and NL-SH parameter sets. The NL1 force does not produce a self-consistent solution for the ground states of C isotopes. We display the energy levels of the triplet of neutron states $1f_{7/2}$, $2p_{3/2}$ and $2p_{1/2}$, the neutron Fermi level and, as reference, the occupied orbital $1d_{3/2}$. Other states in the continuum, as well as deep hole states, are too far away from the Fermi level and therefore not important in the present consideration. Results calculated with different effective interactions are rather similar, and in agreement with our conclusions for Ne isotopes: the location of the neutron drip is essentially determined by the triplet $1f_{7/2}$, $2p_{3/2}$ and $2p_{1/2}$. It appears that NL1 leads to strongest binding, followed by NL3 and NL-SH. For example, ^{28}O is bound for NL1 and NL3,

but unbound for the NL-SH parameter set. As the neutron number $N=20$ is approached, for C, N, O and F the triplet is still high in the continuum, and the pairing interaction does not have enough strength to promote neutrons into these levels. Depending on the effective force, the neutron drip is found at $N=18$ or $N=20$. Starting from Ne, as we have already shown in Fig. 1, the triplet $1f_{7/2}$, $2p_{3/2}$ and $2p_{1/2}$ is much lower and neutrons above $N=20$ begin to fill the $1f_{7/2}$ orbital. For Ne and Na, $2p_{3/2}$ and $2p_{1/2}$ are close to the $1f_{7/2}$, and therefore they are also populated forming the neutron skin, or eventually the neutron halo. For Mg the neutrons above the $s - d$ shell predominantly populate the $1f_{7/2}$ orbital, and one expects that deformation plays an important role in the precise location of the neutron drip.

An interesting result is observed if one plots the neutron single-particle levels as function of the number of protons. This is done in Fig. 5 for $N=18$, $N=20$ and $N=22$ isotones. The levels $2p_{3/2}$, $2p_{1/2}$, $1f_{7/2}$, and $1f_{5/2}$, as well as the neutron Fermi level, are displayed for the three effective forces. For a given number of neutrons, increasing the proton number means going toward the β -stability, i.e. away from the neutron drip-line. The binding increases, as reflected in the negative slope of the Fermi level. What we find very interesting is that the line that corresponds to the Fermi level is almost parallel to the $1f_{7/2}$ level. It appears that the binding of neutrons in these systems is determined by the position of the $1f_{7/2}$ orbital. The levels $2p_{3/2}$, $2p_{1/2}$, and $1f_{5/2}$ change very little with Z . This is also true for $1g_{9/2}$, not shown in the figure, at an energy of ≈ 20 MeV. On the other hand, the energy of the $1f_{7/2}$ orbital decreases considerably by adding more protons. If the spin-orbit splittings are compared, we notice that the energy difference for the doublet $2p_{3/2} - 2p_{1/2}$ is almost constant as function of Z , while a very

strong isospin dependence is observed for $1f_{7/2} - 1f_{5/2}$. This is the crucial point and requires a careful explanation. In Ref. [2] we have analyzed the isospin dependence of the spin-orbit interaction for Ne and Mg isotopes. We have shown that the corresponding term in the potential is strongly reduced when going toward the drip-line. This reduction is especially pronounced in the surface region, and consequently one should observe a more diffuse surface. Since the densities of the f orbitals are located on the surface, while those of the p orbitals are contained in the bulk of the nucleus, the effect of reduction of the spin-orbit interaction will be much stronger for the $1f_{7/2} - 1f_{5/2}$ doublet.

In Fig. 6 we display the neutron densities for the $N=20$ isotones, calculated with the NL3 effective force. The figure corresponds to the central panel in Fig. 5. In the insert of Fig. 6 we include the corresponding values for the surface thickness and diffuseness parameter. The surface thickness s is defined to be the change in radius required to reduce $\rho(r)/\rho_0$ from 0.9 to 0.1 (ρ_0 is the density in the center of the nucleus). The diffuseness parameter α is determined by fitting the neutron density profiles to the Fermi distribution

$$\rho(r) = \rho_0 \left(1 + \exp\left(\frac{r - R_0}{\alpha}\right) \right)^{-1}, \quad (42)$$

where R_0 is the half-density radius. In going away from the drip line, from ^{28}O to ^{32}Mg , the surface thickness decreases from 2.8 fm to 2.33 fm, and the diffuseness parameter decreases from 0.64 fm to 0.55 fm. We have shown the vector densities. However, the scalar densities display the same radial dependence. This means that the scalar potential S and the vector potential V behave in the same way in the surface region, i.e. both potentials display the same diffuseness.

These large changes in surface properties reflect the reduction of the spin-orbit term of the potential. In relativistic mean-field approximation, the spin-orbit potential originates from the addition of two large fields: the field of the vector mesons (short range repulsion), and the scalar field of the sigma meson (intermediate attraction). In the first order approximation, and assuming spherical symmetry, the spin orbit term can be written as

$$V_{s.o.} = \frac{1}{r} \frac{\partial}{\partial r} V_{ls}(r), \quad (43)$$

where V_{ls} is the spin-orbit potential [8, 21]

$$V_{ls} = \frac{m}{m_{eff}}(V - S). \quad (44)$$

V and S denote the repulsive vector and the attractive scalar potentials, respectively. m_{eff} is the effective mass

$$m_{eff} = m - \frac{1}{2}(V - S). \quad (45)$$

Using the vector and scalar potentials from the NL3 self-consistent ground-state solutions, we have computed from (43) - (45) the spin-orbit terms for the N=20 isotones. They are displayed in Fig. 7 as function of the radial distance from the center of the nucleus. The magnitude of the spin-orbit term $V_{s.o.}$ increases as we add more protons, i.e. as we move away from the drip-line. In Fig. 8 we also plot the proton and neutron *rms* radii for the N=20 isotones, calculated with all three parameter sets. The results are very similar, and show how the neutron radii decrease in going toward the stability line. At the same time, of course, the proton radii increase.

Finally, in Fig. 9 we compare the neutron *rms* radii for Na isotopes with recent experimental data from Ref. [22]. Theoretical values correspond to ground-state densities calculated with the NL3 effective interaction, and

the D1S parameters for the Gogny interaction in the pairing channel. The blocking procedure has been used both for protons and neutrons. With the possible exceptions of $N=11$, the theoretical values nicely reproduce the experimental data, much better than the RMF parameter set that has been used in Ref. [22]. The neutron *rms* radii display a uniform increase. Unlike in the case of Ne, no sudden change in the radii is observed. Instead of the neutron halo, what we observe in Na isotopes is more probably the formation of the neutron skin. In fact, in the insert of Fig. 9 we display the calculated and experimental differences between neutron and proton radii. The smooth increase of $r_n - r_p$ after $N=11$ presents evidence for a large neutron skin. Of course, this does not prevent the formation of the halo for heavier Na isotopes. The discrepancy of the calculated and measured r_n for $N=11$ probably comes from the fact that for this isotope the proton and neutron numbers are identical, and therefore both the odd proton and odd neutron occupy the $s - d$ orbitals with the same probabilities. One should expect a short range interaction, possibly proton-neutron pairing. Such an interaction would lower the total energy, and the resulting radius should be smaller. An explicit proton-neutron interaction is not included in the theoretical model, and therefore the calculated neutron radius is larger than the experimental value.

4 Conclusions

In the present work we have investigated properties of light nuclei with large neutron excess. Neutron-rich nuclei between Carbon and Magnesium have recently become available in experiments with radioactive nuclear beams, and therefore it is very important to study the properties that various the-

oretical models predict for this region. We have calculated ground state properties using the Relativistic Hartree Bogoliubov theory. Based on the relativistic mean-field model on one side, and the HFB theory on the other, RHB provides a unified description of mean-field and pairing correlations. It describes the nucleus as a relativistic system of baryons and fermions. Pairing correlations are described by finite range two-body forces. Very little is known about the pp component of the effective interaction in relativistic models, and therefore we have used a finite range interaction of Gogny-type. Finite element methods have been used in the coordinate space discretization of the coupled system of Dirac-Hartree-Bogoliubov integro-differential eigenvalue equations, and Klein-Gordon equations for the meson fields. Coordinate space solutions are essential for a correct description of particle-hole and pair excitations into the continuum. For the mean-field Lagrangian we have used the well established effective interactions NL1, NL3 and NL-SH, and the D1S parameter set for the finite range Gogny type interaction in the pairing channel. In particular, we have investigated the location of the neutron drip-line as function of the number of protons.

Model calculations have shown that the triplet of single-particle states near the neutron Fermi level: $1f_{7/2}$, $2p_{3/2}$ and $2p_{1/2}$, and the neutron pairing interaction determine the location of the neutron drip-line, the formation of the neutron skin, or eventually of the neutron halo. For C, N, O and F the triplet is still high in the continuum at $N=20$, and the pairing interaction is too weak to promote pairs of neutrons into these levels. All mean-field effective interactions predict similar results, and the neutron drip is found at $N=18$ or $N=20$. For Ne, Na, and Mg the states $1f_{7/2}$, $2p_{3/2}$ and $2p_{1/2}$ are much lower in energy, and for $N \geq 20$ the neutrons populate these levels. The neutron drip

can change by as much as twelve neutrons. The model predicts the formation of neutron skin, and eventually neutron halo in Ne and Na. This is due to the fact that the triplet of states is almost degenerate in energy for $N \geq 20$. For Mg the $1f_{7/2}$ lies deeper and neutrons above the $s - d$ shell will exclusively populate this level, resulting in a deformation of the mean field. When we plot the neutron single-particle levels as function of the number of protons, it turns out that the binding of neutrons is determined by the $1f_{7/2}$ orbital which is found to be parallel to the slope of the Fermi level. The reduction of the spin-orbit splitting $1f_{7/2} - 1f_{5/2}$ close to the neutron-drip line has been related to the isospin dependence of the spin-orbit interaction. Density distributions have been analyzed, and the resulting surface thickness and diffuseness parameter reflect the reduction of the spin-orbit term of the effective potential in the surface region of neutron-rich nuclei. Model calculations reproduce the recent experimental data on the neutron *rms* radii for Na isotopes.

The results of the present work clearly show that a correct theoretical description of nuclei with large neutron excess necessitates the following essential ingredients:

- i) self-consistent solution for the mean-field in order to obtain the correct increase of the surface diffuseness,
- ii) the correct isospin dependence of the spin-orbit term in the mean-field potential. At present only relativistic models provide reliable results for the characteristic spacings of single particle levels at the Fermi surface.
- iii) pairing correlations describe the scattering of nucleon pairs for states close to the Fermi surface. Pairing leads to the partial occupation of single particle levels with low orbital angular momentum.

iv) pairing correlations in the continuum should be described by RHB in coordinate space, with finite-range pairing interaction. In this procedure the scattering of nucleon pairs does not lead to unbound configurations.

Thus Relativistic Hartree-Bogoliubov theory in coordinate space provides an appropriate framework in which properties of exotic nuclei on both sides of the valley of β -stability can be studied. However, to calculate ground-state properties of heavier nuclei beyond Na or Mg, deformations of the mean-field have to be taken into account. The inclusion of deformation in the coordinate space formulation of RHB with finite range pairing still presents considerable difficulties. It is also clear that the details of the scattering processes around the Fermi surface, and the partial occupation of levels with low orbital angular momentum in the continuum, are determined by the strength and functional dependence of pairing correlations. As long as a fully microscopic derivation of an effective pairing in nuclei is not available, it is justified to use a phenomenological interaction, as for example the Gogny force. Another open problem is whether one needs a density dependent pairing interaction.

References

- [1] W. Pöschl, D. Vretenar, G.A. Lalazissis, and P. Ring, Phys. Rev. Lett. (1997).
- [2] G.A. Lalazissis, D. Vretenar, W. Pöschl, and P. Ring, Phys. Lett. **B** (1997).
- [3] W. Pöschl, D. Vretenar, A. Rummel, and P. Ring; Comput. Phys. Commun. **101** (1997) 75.
- [4] W. Pöschl, D. Vretenar and P. Ring; Comput. Phys. Commun. (1997)
- [5] B.D. Serot and J.D. Walecka; Adv. Nucl. Phys. **16** (1986) 1.
- [6] P.G. Reinhard; Rep. Prog. Phys. **52** (1989) 439.
- [7] B.D. Serot; Rep. Prog. Phys. **55** (1992) 1855.
- [8] P. Ring; Progr. Part. Nucl. Phys. 37 (1996) 193.
- [9] J. Boguta and A.R. Bodmer; Nucl. Phys. A292 (1977) 413
- [10] Y.K. Gambhir, P. Ring, and A. Thimet; Ann. Phys. (N.Y.) **511** (1990) 129.
- [11] J. Dobaczewski, H. Flocard, and J. Treiner; Nucl. Phys. **A422** (1984) 103.
- [12] J. Dobaczewski, W. Nazarewicz, T. R. Werner, J. F. Berger, C. R. Chinn, and J. Dechargé; Phys. Rev. **C53** (1996) 2809.
- [13] P. Ring, and P. Schuck; "The Nuclear Many-Body Problem" (Springer-Verlag, Heidelberg 1980).

- [14] H. Kucharek and P. Ring; Z. Phys.. **A 339** (1991) 23.
- [15] P.G. Reinhard, M.Rufa, J. Maruhn, W. Greiner and J. Friedrich; Z. Phys. **A 323** (1986) 13.
- [16] G.A. Lalazissis, J. König, and P. Ring; Phys. Rev. C **55** (1997) 540.
- [17] M.M. Sharma, M.A. Nagarajan, and P. Ring; Phys. Lett. **B312** (1993) 377.
- [18] J. F. Berger, M. Girod and D. Gogny; Nucl. Phys. **A428** (1984) 32.
- [19] J. Meng and P. Ring; Phys. Rev. Lett. 77 (1996) 3963.
- [20] J. Meng and P. Ring; Phys. Rev. Lett. (1997)
- [21] W. Koepf and P. Ring; Z. Phys. **A339** (1991) 81.
- [22] T. Suzuki et al., Phys. Rev. Lett. **75** (1995) 3241.

Figure Captions

Fig.1 Calculated proton and neutron *rms* radii for Ne isotopes (a), and the 1f-2p single-particle neutron levels in the canonical basis (b).

Fig.2 The neutron single-particle levels $1d_{3/2}$, $1f_{7/2}$, $2p_{3/2}$ and $2p_{1/2}$ for N, O, and F isotopes. Solid lines denote the neutron Fermi level. The energies correspond to ground-state solutions calculated with the NL1, NL3 and NL-SH effective forces of the mean-field Lagrangian. The parameter set D1S is used for the finite range Gogny-type interaction in the pairing channel.

Fig.3 Same as in Fig. 2, but for the isotopes of Ne, Na and Mg.

Fig.4 Same as in Fig. 2, but for C isotopes and the NL3 and NL-SH effective interactions.

Fig.5 The neutron single-particle levels $2p_{3/2}$, $2p_{1/2}$, $1f_{7/2}$, and $1f_{5/2}$ for the N=18, N=20 and N=22 isotones, as function of the proton number. Solid lines denote the neutron Fermi level. The first, second and third row correspond to calculations performed with the NL1, NL3 and NL-SH effective forces, respectively.

Fig.6 Neutron density distributions for the N=20 isotones, calculated with the NL3 effective force. In the insert the corresponding values for the surface thickness and diffuseness parameter are included.

Fig.7 Radial dependence of the spin-orbit term in self-consistent solutions for the ground-states of the N=20 isotones, calculated with the NL3 effective force.

Fig.8 Proton and neutron *rms* radii for the N=20 isotones. The panels correspond to results obtained with the NL1, NL3 and NL-SH effective forces, respectively.

Fig.9 Comparison of the neutron *rms* radii for Na isotopes with experimental data from Ref. [22]. Theoretical values (squares) correspond to ground-state densities calculated with the NL3 effective interaction. The calculated differences between neutron and proton radii are displayed in the insert.

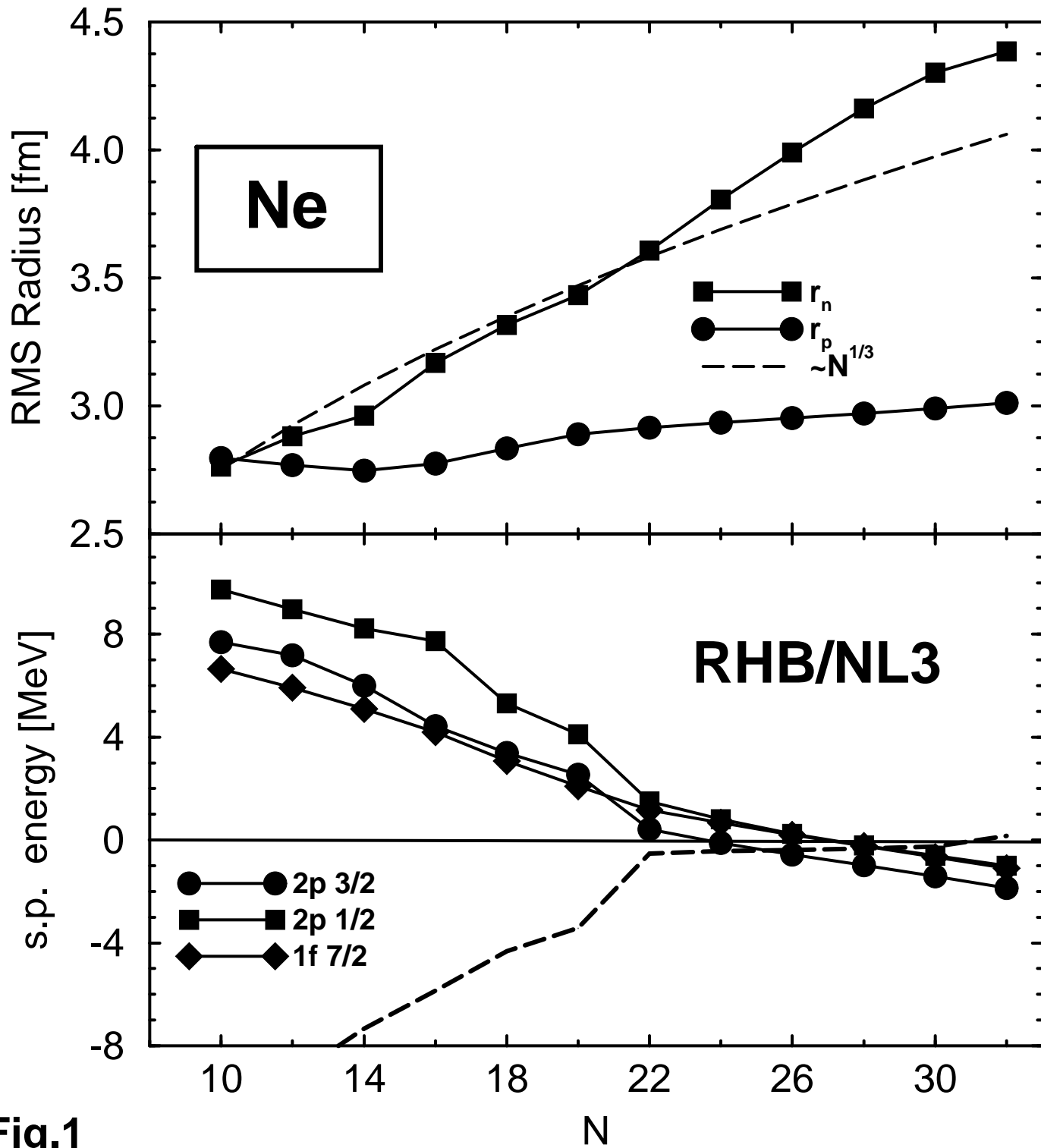


Fig.1

s.p. energy [MeV]

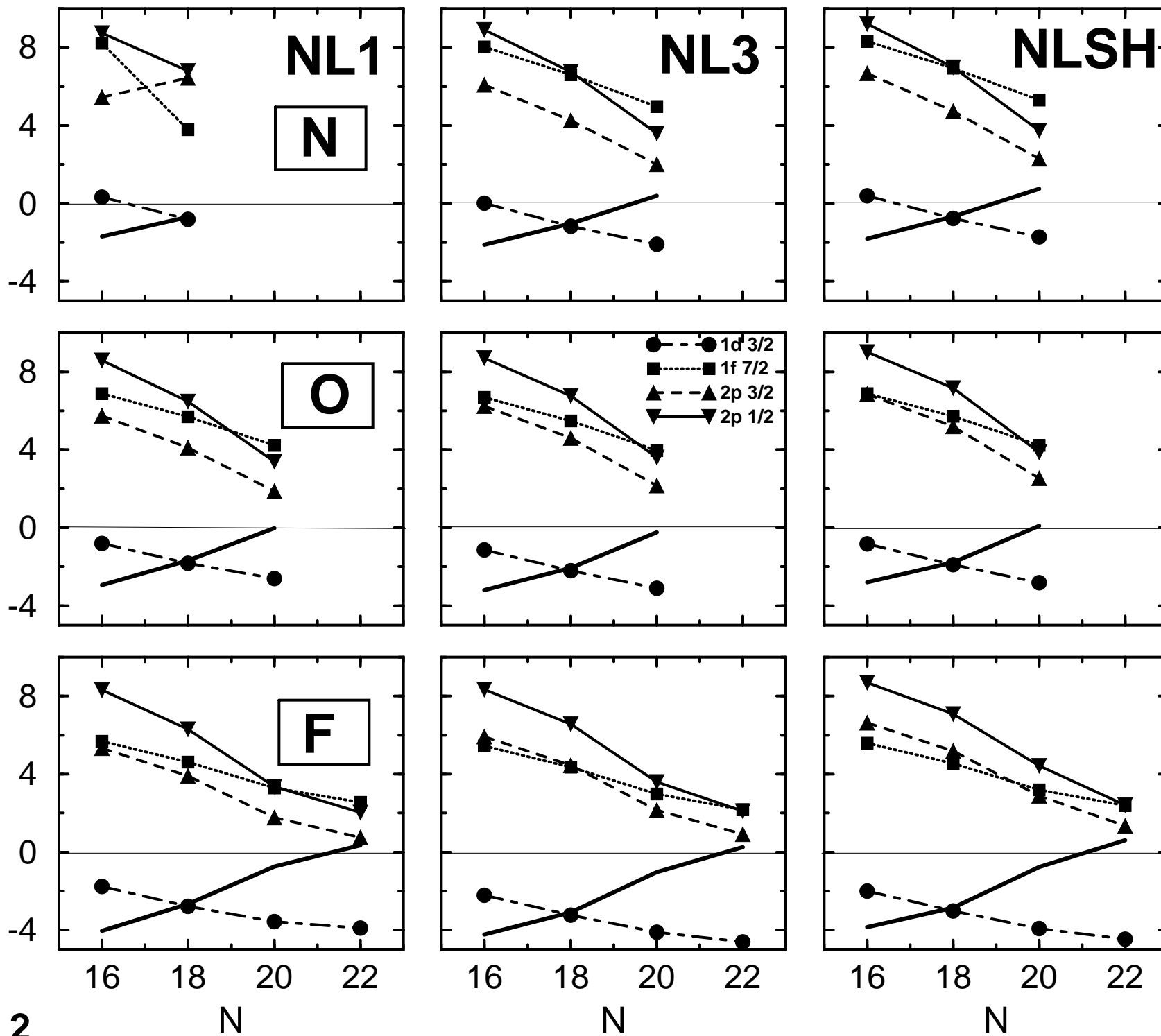


Fig. 2

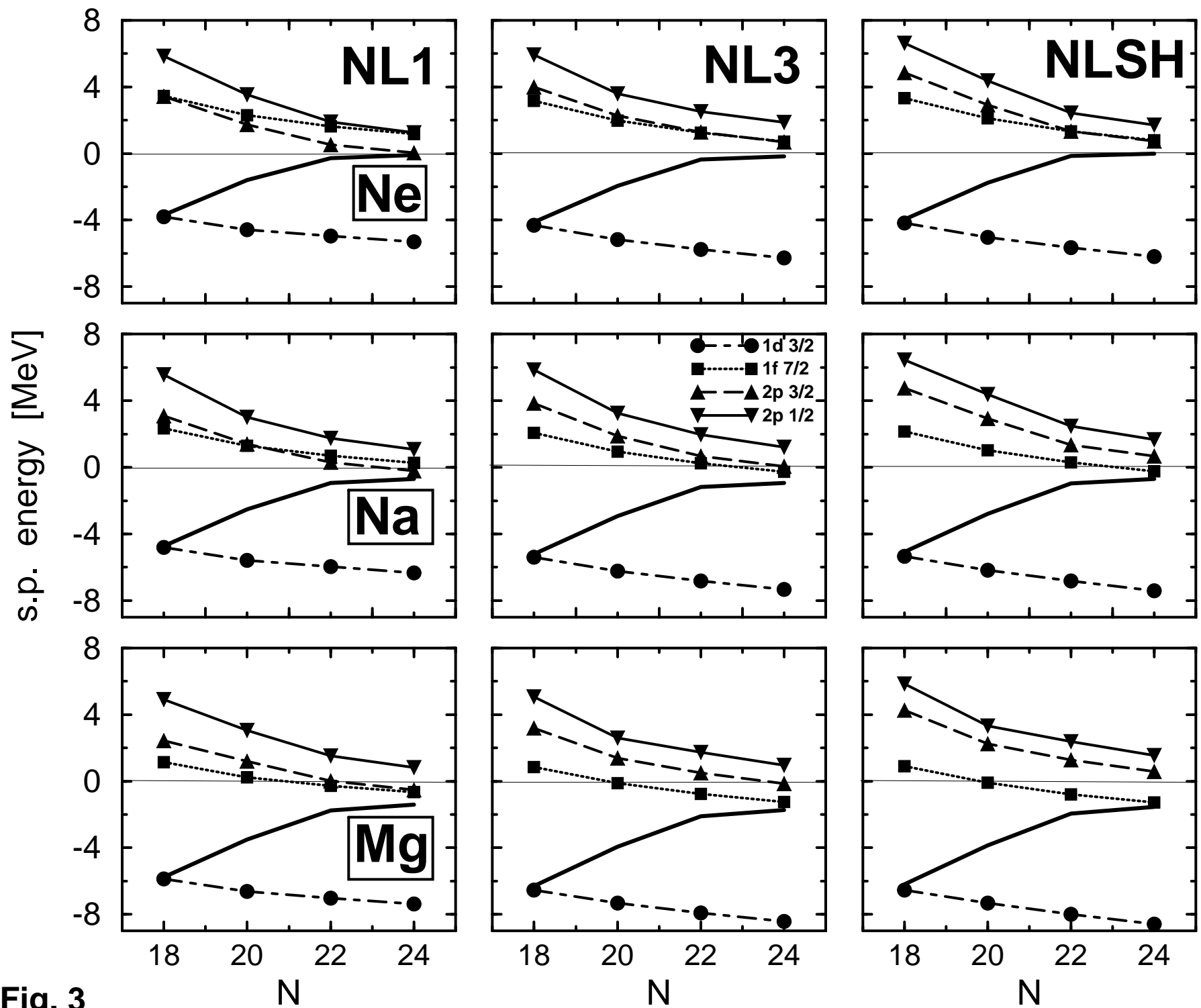


Fig. 3

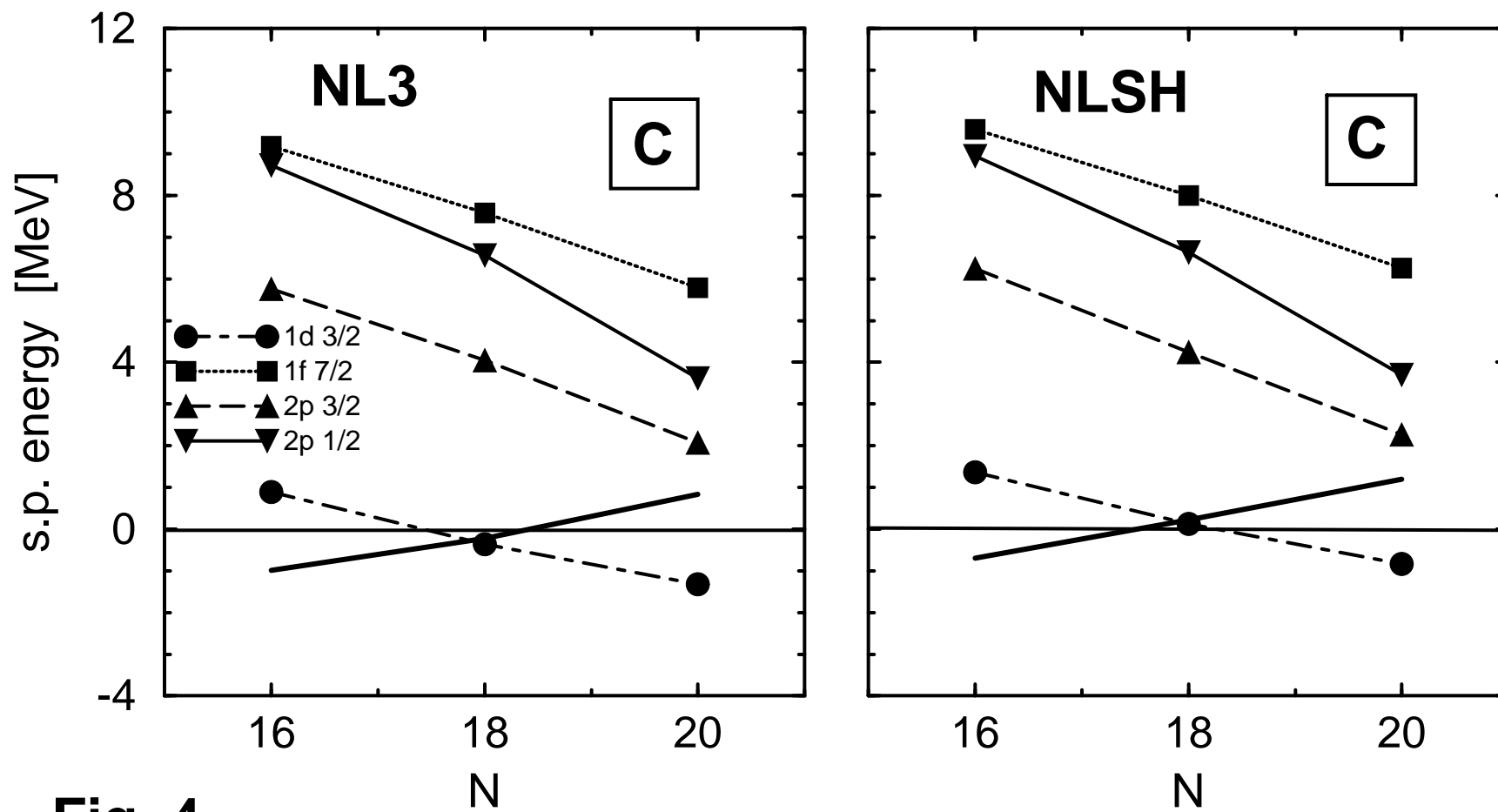


Fig. 4

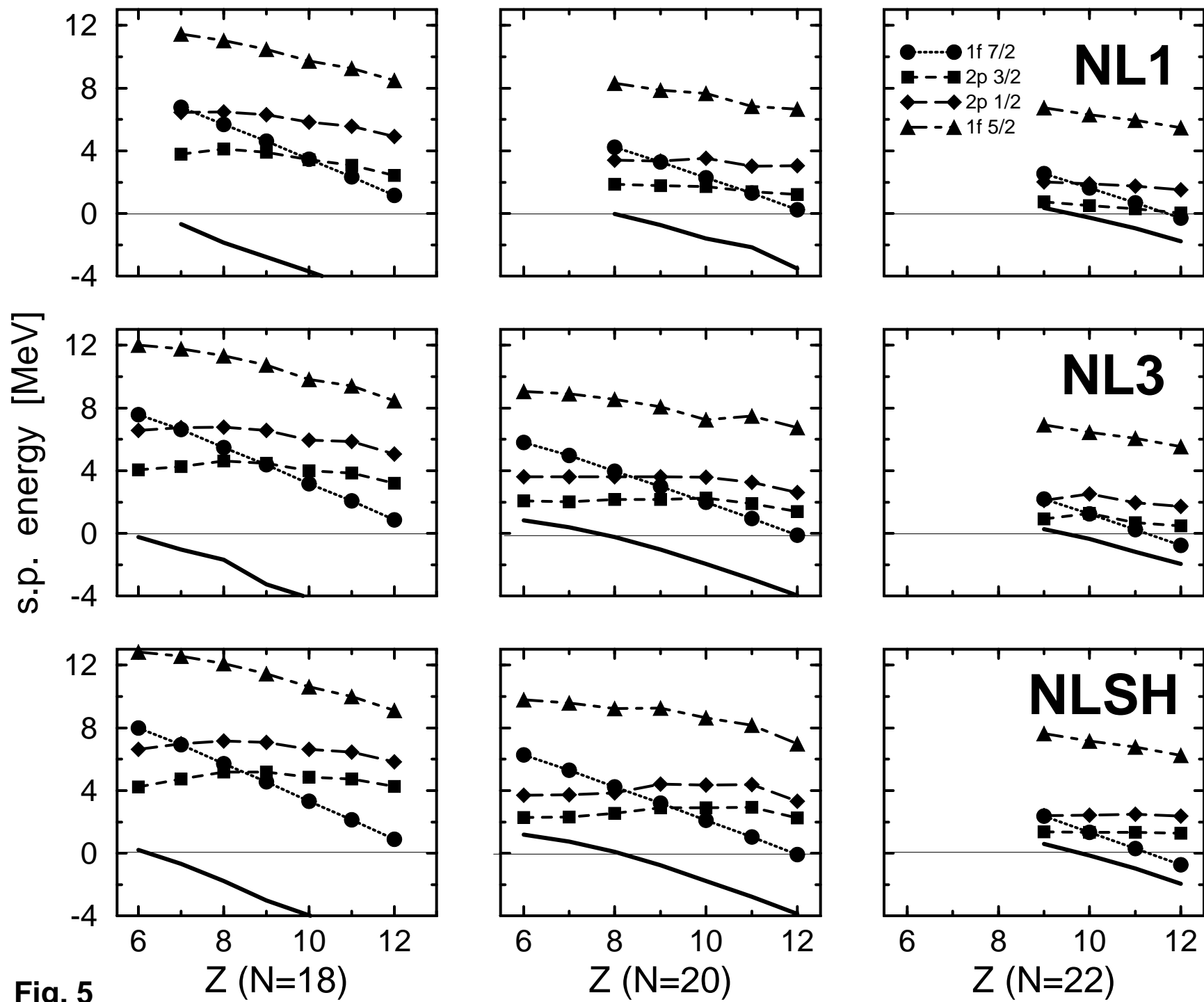


Fig. 5

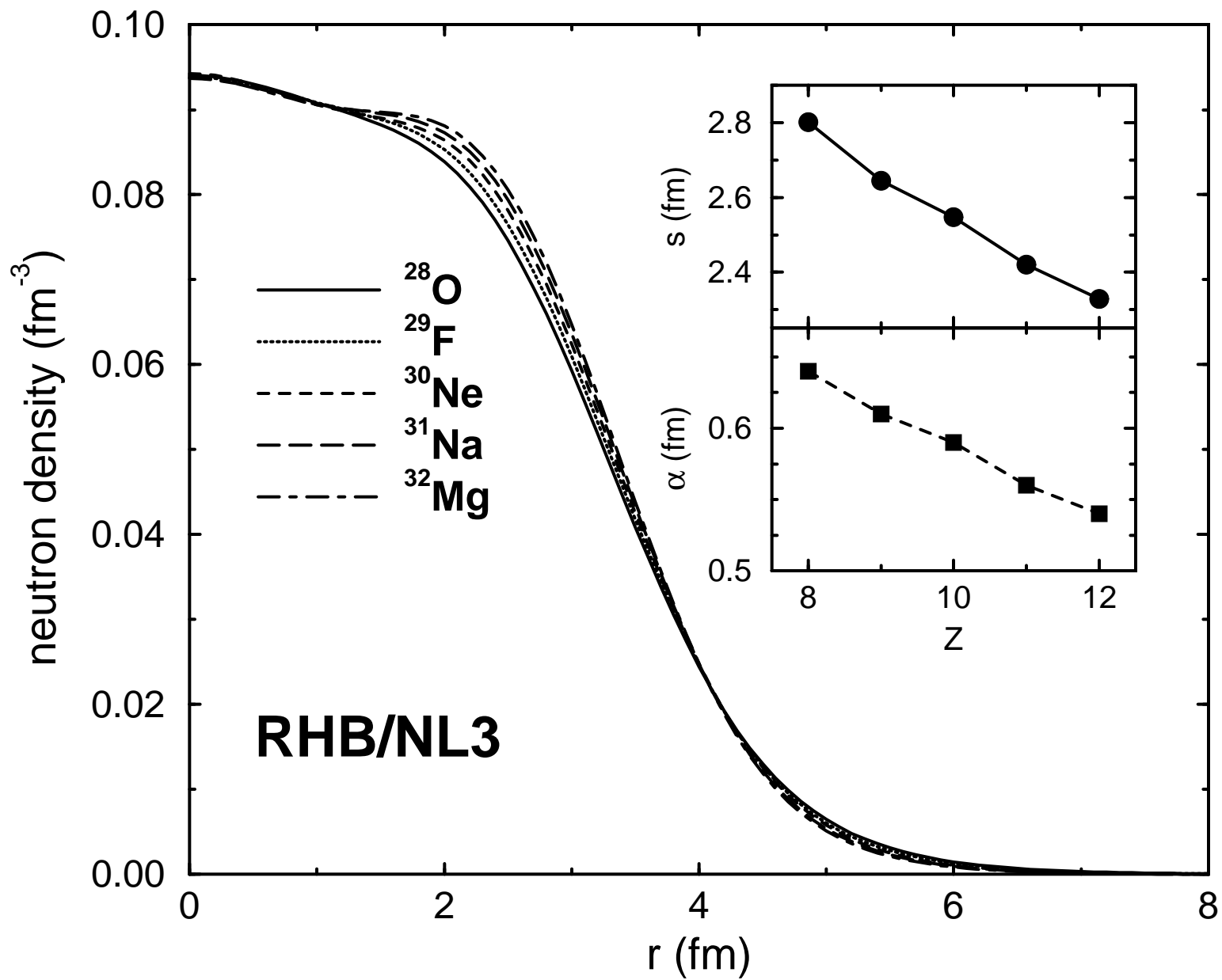


Fig. 6

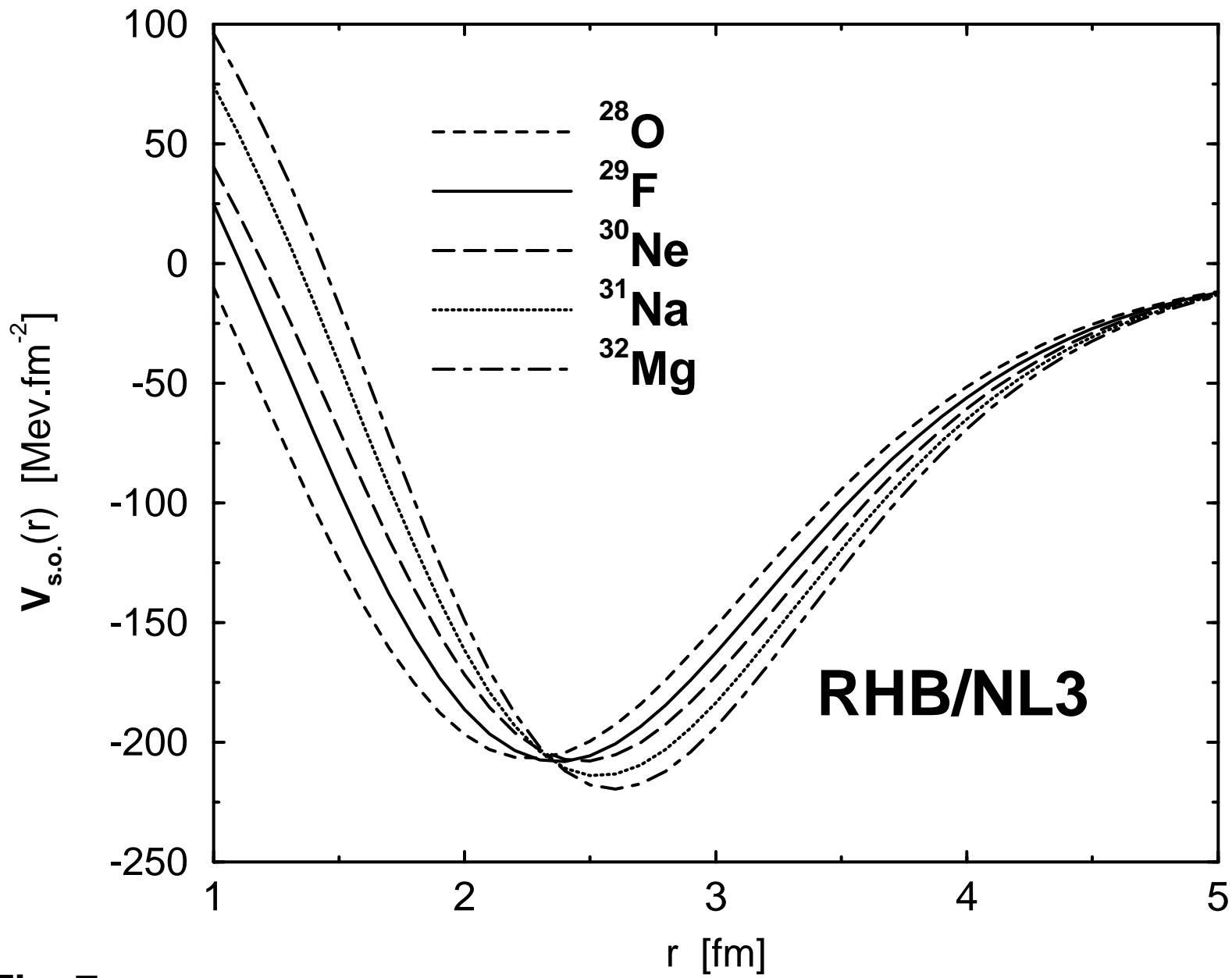


Fig. 7

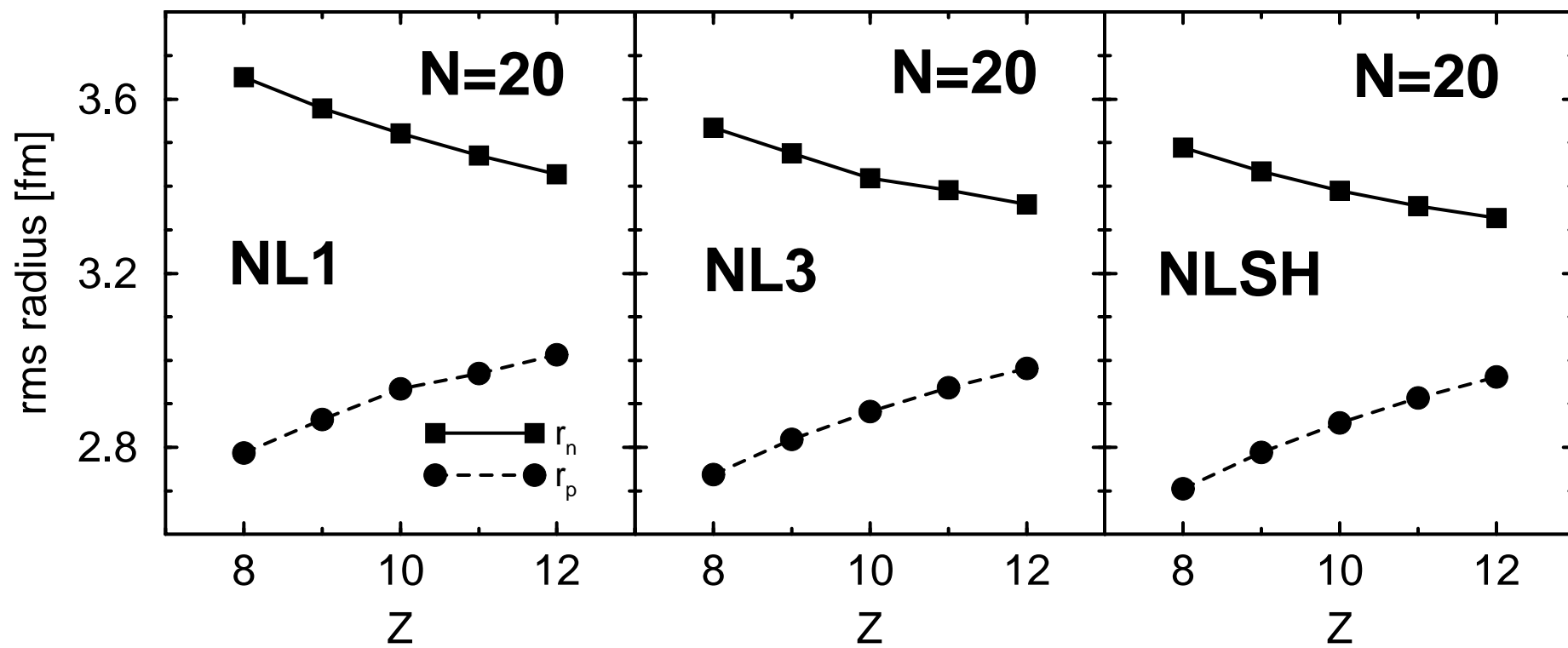


Fig. 8

Fig. 9

